Full Paper

Modelling of a high-speed precision robot for microelectro-mechanical systems bonding process application

Anees A. Sneineh and Wael A. Salah[*]

Department of Electrical Engineering, College of Engineering and Technology, Palestine Technical University - Kadoorie, P.O.Box 7, Yafa Street, Tulkarm, Palestine

* Corresponding author, e-mail: wael.salah@ptuk.edu.ps; waelsalah.dr@gmail.com

Abstract: This paper presents the modelling of a planar parallel manipulator with two degrees of freedom by performing analyses of workspace, velocity and precision. Given that microelectromechanical systems (MEMS) are essential in the integration of mechanical system applications, the automation of the robot to be used for MEMS bonding process applications is proposed. This type of manipulator is commonly used for assembling electronic devices and in MEMS bonding because of its advantages over the serial manipulator. Forward and inverse kinematics and trajectory generation are determined. Singularity and workspace analyses are performed and dynamic equations for the actuators are determined. A control system is constructed by using a motion control card and motor driver amplifier to meet the requirements of the MEMS industry. Experimental results prove that the robot works in real time with high speed and high acceleration and presents a good response to trajectory generation. The robot covers the workspace field and avoids singularity.

Keywords: microelectromechanical systems, planar parallel manipulator, kinematics, singularity, motion control

INTRODUCTION

Determination of the workspace area expression of planar parallel manipulators has been presented [1] to optimise and develop the design of these manipulators, and workspace analysis was carried out by using a non-dimensional approach. Workspace shape was classified as a function of geometric parameters and closed-form area expressions were derived for a constant orientation workspace of a three–revolute–revolute–revolute planar manipulator [1]. Another study presented

the design criteria based on dynamic and elastodynamic models of planar parallel mechanisms. Dynamic performance was evaluated by using global dynamic dexterity [2].

Microelectromechanical systems (MEMS) involve the integration of mechanical elements, sensors, actuators and integrated circuits (IC) into a common silicon substrate through microfabrication. MEMS promise to revolutionise nearly every product category by bringing together silicon-based microelectronics and micromachining technology, thus facilitating the realisation of complete systems on chip. MEMS are a technology that allows the development of smart products, augments the computational capability of microelectronics with the perception and control capabilities of microsensors and microactuators, and expands the scope of possible designs and applications [3-8].

Given that MEMS devices are manufactured through batch fabrication techniques [6-8], unprecedented levels of functionality, reliability and sophistication can be placed on a small silicon chip at a relatively low cost. MEMS are important in life and automation applications. Therefore, the proposed robot was developed and assembled through IC and MEMS bonding. The MEMS and IC bond require high speed, high precision and a small workspace. A parallel robot can meet these requirements. Therefore, this paper presents the development of a modular high-speed, high-precision planar parallel robot with two degrees of freedom (DOF).

A platform is primarily required which contains the gold wire and connects it to the sensor inside the chip to build the IC, as shown in Figure 1.
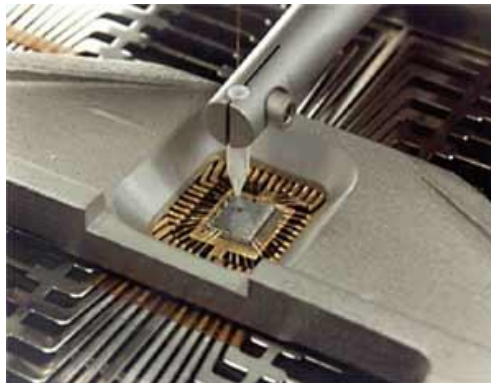

Figure 1. IC and MEMS bonding process

In this research the experimental results prove that the robot works in real time with high speed and high acceleration. The structural design of the proposed robot aims to eliminate several singularities that limit the robot workspace through the existence of the parallelogram part. Most singularities cannot occur due to several mechanical constraints. Nevertheless, several singularity conditions in the workspace of the robot still occur. This issue can be resolved during the design and implementation of the control part of the proposed robot, which can successfully avoid singularities and allow for the covering of the workspace field. The proposed design of the robot manipulator presents advantages in terms of shape and geometry compared with existing planner robots. This design enables high flexibility that makes the proposed design suitable for fulfilling the required application in MEMS bonding. In addition, the proposed design shows a good response to trajectory generation.

MECHANICAL STRUCTURE

Parallel manipulators are important for the manipulation and assembly of IC [9] and MEMS bonding and manufacturing. The proposed 2-DOF planar parallel manipulators possess a high ratio of stiffness to mass and can easily obtain high speed and high acceleration. As shown in Figure 2, the proposed manipulator is composed of three parts: a planar parallel manipulator with its parallelogram part, a linear actuator module (end-effector), and two actuators (motors).

(a) Proposed robot   (b) Prototype robot
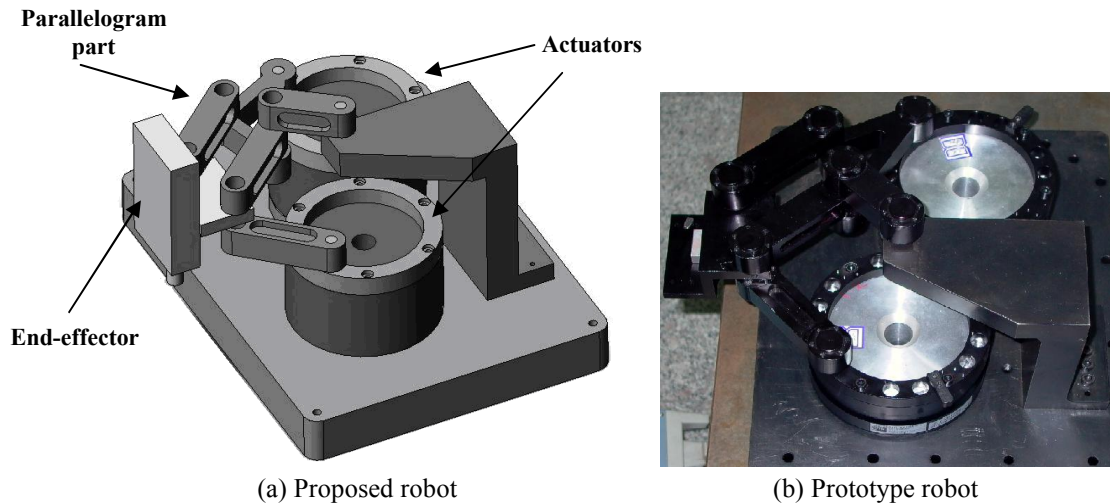
Figure 2. 2-DOF planar parallel manipulator

The function of the parallelogram part is to improve the stiffness of the manipulator in the vertical direction and constrain the rotational motion of the end-effector [10], which limits the application of the conversional planar parallel manipulator and makes position measurement difficult. It also provides the opportunity for some singularities to occur in the workspace [11-14].

Compared with a parallel manipulator with high degrees of freedom, kinematic and dynamic models of the planar parallel manipulator are simple [15-16], and this simplicity makes real-time control possible and precise [17-19]. Compared with the serial manipulator, a parallel manipulator has high stiffness because of its closed-loop feature and low moment of inertia since the driver parts are placed on the base [20-22]. The driver device serves as the load of the preceding stage in the serial structure.

Direct drive is another advantage of the manipulator. The system overcomes mechanical elasticity because flex coupling, gear teeth, bearing, bearing support, connecting shaft and other parts are included in the classical drive system. Therefore, this manipulator can easily obtain a good dynamic performance and high precision. In this study, two AC direct-driven motors integrated with a high-resolution encoder were selected as the driven part.

The linear actuator module is also directly driven by the voice coil motor, which is considered an ideal driving component for short travel. As a non-commutated, direct-drive, hysteresis-free, cog-free device, the voice coil motor can provide high position sensitivity and perfect force-versus-stroke character. High-precision linear encoders are used as feedback parts to guarantee repeatability in the vertical direction.

KINEMATIC MODEL

Research on kinematic analysis includes forward and inverse kinematics [23-26]. Forward displacement analysis requires the determination of the end-effector pose given the actuated joint displacements. Establishing an efficient solution to the forward displacement problem is fundamental in a successful implementation of robotic devices. A duality problem, in which a difficult problem for one is easily solved for the other, exists between parallel and serial mechanisms. Forward displacement analysis for parallel mechanisms is a difficult analytical problem that involves solving non-linear equations that result in multiple solutions. By contrast, inverse kinematic analysis is generally an easier problem.

This section presents the homogeneous transformation matrices and geometrical analytical method required to describe the relative position and orientation between the coordinate frames and the robot base. The trajectory [22] for the two actuators and the displacement for the end-effector are also presented.

Forward Kinematics

Forward kinematics helps calculate the position and orientation of the platform (end-effector) when the lengths of the links are provided [23]. A 2-DOF planar parallel manipulator and its coordinate system definition are shown in Figure 3, where θ_1 and θ_2 are the driving angles for inputs, B and D are passive joint angles, and e is the distance from the origin of the base to joint A or to joint E. The length of each link is also shown in the figure.
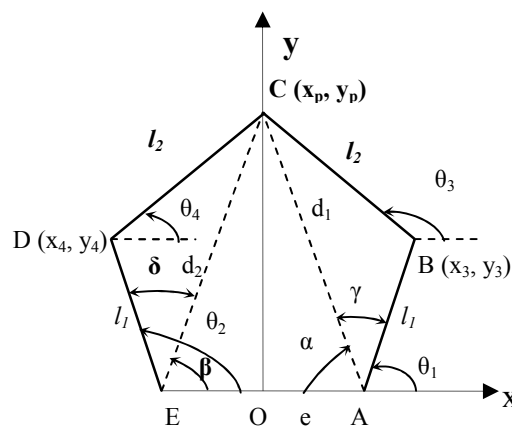
Figure 3. Five-link structure and definition of coordinate systems (See description of parameters in Appendix.)

The homogeneous transformation matrices for the first and second links are established from Figure 3 as follows:

$$
{}^{0}T_{1} = \begin{bmatrix} \cos(\theta_1) & -\sin(\theta_1) & 0 & e \\ \sin(\theta_1) & \cos(\theta_1) & 0 & 0 \\ 0 & 0 & 1 & 0 \\ 0 & 0 & 0 & 1 \end{bmatrix}, \qquad (1)
$$

$$^0T_2 = \begin{bmatrix} \cos(\theta_2) & -\sin(\theta_2) & 0 & -e \\ \sin(\theta_2) & \cos(\theta_2) & 0 & 0 \\ 0 & 0 & 1 & 0 \\ 0 & 0 & 0 & 1 \end{bmatrix}. \tag{2}$$

The coordinate position of points B and D are determined. Afterward, the homogeneous transformation matrices for the third and fourth links are established. The coordinates for joint B are located at $x_3 = e + l_1 \cos(\theta_1)$ and $y_3 = l_1 \sin(\theta_1)$, and the coordinates for joint D are located at $x_4 = -e + l_1 \cos(\theta_2)$ and $y_4 = l_1 \sin(\theta_2)$. The distance between points B and D in Figure 3 is $d_{34} = \sqrt{(x_3 - x_4)^2 + (y_3 - y_4)^2}$.

Angles θ_3 and θ_4 are the orientation angles of the third and fourth links respectively in the base coordinate system and can be defined as follows:

$$\theta_3 = \pi + \tan^{-1}\left(\frac{y_3 - y_4}{x_3 - x_4}\right) - \cos^{-1}\left(\frac{d_{34}}{2l_2}\right), \tag{3}$$

$$\theta_4 = \tan^{-1}\left(\frac{y_3 - y_4}{x_3 - x_4}\right) + \cos^{-1}\left(\frac{d_{34}}{2l_2}\right). \tag{4}$$

After defining θ_3 and θ_4 in equations 3 and 4 respectively, the homogeneous transformation matrices for the third and fourth links are established as follows:

$$^0T_3 = \begin{bmatrix} \cos(\theta_3) & -\sin(\theta_3) & 0 & x_3 \\ \sin(\theta_3) & \cos(\theta_3) & 0 & y_3 \\ 0 & 0 & 1 & 0 \\ 0 & 0 & 0 & 1 \end{bmatrix}, \tag{5}$$

$$^0T_4 = \begin{bmatrix} \cos(\theta_4) & -\sin(\theta_4) & 0 & x_4 \\ \sin(\theta_4) & \cos(\theta_4) & 0 & y_4 \\ 0 & 0 & 1 & 0 \\ 0 & 0 & 0 & 1 \end{bmatrix}. \tag{6}$$

To determine the position of joint C (end-effector), we approach the geometric expressions from two branches, namely A-B-C and E-D-C. The coordinates for joint C are located at (x_p, y_p), which can be defined as follows:

$$\left.\begin{array}{l} y_p = \dfrac{-b \pm \sqrt{b^2 - 4ac}}{2a}, \\[2mm] x_p = Ky + W \end{array}\right\} \tag{7}$$

where $a = 1 + K^2$, $\qquad b = 2K(W - x_1) - 2y_1$,

$c = (W - x_1)^2 + y_1^2 - l_2^2$, $\qquad K = \dfrac{y_1 - y_2}{x_2 - x_1}$, $\qquad W = \dfrac{x_2 + x_1}{2} + \dfrac{y_2^2 - y_1^2}{2(x_2 - x_1)}$

and (x_1, y_1) and (x_2, y_2) are the coordinate position for points A and E respectively.

Alternatively, the position of the coordinate can be obtained easily by using homogeneous transformation matrices $^0T_3$ multiplied by the length vector of the third link as follows:

$$\begin{bmatrix} x_p \\ y_p \end{bmatrix} = {}^0T_3 \begin{bmatrix} l_2 \\ 0 \\ 0 \\ 1 \end{bmatrix} = \begin{bmatrix} l_2 \cos(\theta_3) + x_3 \\ l_2 \sin(\theta_3) + y_3 \end{bmatrix}. \tag{8}$$

Similarly, we determine the homogeneous transformation matrices for the fifth, sixth and seventh links. The mechanical structure of the manipulator and the definition of several additional link coordinate systems are shown in Figure 4. The known lengths of sides BF, FG and BG are l_3, l_4 and l_5 respectively.

The orientation angle of the sixth link is also θ_3. The defined θ_5 and θ_7 are the orientation angles of links 5 and 7 respectively. Therefore, we have

$$^0T_5 = \begin{bmatrix} \cos(\theta_5) & -\sin(\theta_5) & 0 & x_3 \\ \sin(\theta_5) & \cos(\theta_5) & 0 & y_3 \\ 0 & 0 & 1 & 0 \\ 0 & 0 & 0 & 1 \end{bmatrix}, \tag{9}$$

$$^0T_6 = \begin{bmatrix} \cos(\theta_3) & -\sin(\theta_3) & 0 & x_6 \\ \sin(\theta_3) & \cos(\theta_3) & 0 & y_6 \\ 0 & 0 & 1 & 0 \\ 0 & 0 & 0 & 1 \end{bmatrix}, \tag{10}$$

$$^0T_7 = \begin{bmatrix} \cos(\theta_7) & -\sin(\theta_7) & 0 & x_p \\ \sin(\theta_7) & \cos(\theta_7) & 0 & y_p \\ 0 & 0 & 1 & 0 \\ 0 & 0 & 0 & 1 \end{bmatrix}. \tag{11}$$
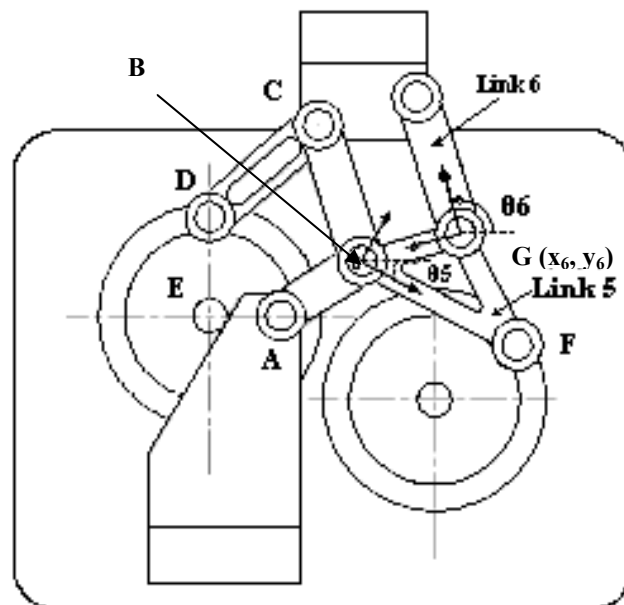
Figure 4. Mechanical structure of the manipulator (See description of parameters in Appendix.)

The constant θ_5 is determined by the geometrical configuration, and θ_7 is always equal to zero because of the special structural configuration.

The geometric coordinate of joint 6 (x_6, y_6) are also determined by θ_1, θ_2 and several known parameters as: $x_6 = x_3 + l_5 \cos(\theta_t)$ and $y_6 = y_3 + l_5 \sin(\theta_t)$, where $\theta_t = \cos^{-1}\left(\dfrac{l_3^2 + l_5^2 - l_4^2}{2l_3 l_5}\right)$ and θ_t is the orientation angle of segment BG in the base coordinate system, which is also a constant. The position and orientation of all the links in the robot are now known.

Inverse Kinematics

The purpose of inverse kinematics is to determine the input joint values when the desired pose of the end-effector is provided [24]. Therefore, we determine θ_1 and θ_2 by using the values of the position of the end-effector. From the distance between the first joint and the reference point on the manipulating platform (points A and C) in Figure 4, we derive

$$d_1 = \sqrt{(x_p - e)^2 + y_p^2} \ . \tag{12}$$

Similarly, the distance between the second joint and the reference point on the manipulating platform (points E and C) is

$$d_2 = \sqrt{(x_p + e)^2 + y_p^2} \ . \tag{13}$$

To obtain angles γ and δ we apply cosine law on triangle ABC, as shown in equations 14 and 15:

$$\gamma = \cos^{-1}\left(\frac{d_1^2 + l_1^2 - l_2^2}{2d_1 l_1}\right) \quad (0 < \gamma < \pi), \tag{14}$$

$$\delta = \cos^{-1}\left(\frac{d_2^2 + l_1^2 - l_2^2}{2d_2 l_1}\right) \quad (0 < \delta < \pi). \tag{15}$$

Inside triangle ACE, by applying the cosine law we obtain angles α and β as shown in equations 16 and 17:

$$\alpha = \cos^{-1}\left(\frac{4e^2 + d_1^2 - d_2^2}{4d_1 e}\right) \ , \tag{16}$$

$$\beta = \cos^{-1}\left(\frac{4e^2 + d_2^2 - d_1^2}{4d_2 e}\right) \ . \tag{17}$$

Therefore, we obtain the angle value of input joints θ_1 and θ_2 as in equations 18 and 19:

$$\theta_1 = \pi - \alpha - \gamma \ , \tag{18}$$
$$\theta_2 = \beta + \delta \ . \tag{19}$$

The inverse kinematics of the robot is then determined.

Trajectory Generation

A trajectory generation curve for the actuators can be obtained (Figure 5) by using the inverse kinematic solution of θ_1 and θ_2 from equations 18 and 19 respectively, then selecting different angles of α, β, γ and δ within the workspace area, and implementing θ_1 and θ_2 by the MATLAB

program with respect to time. Figure 5 shows that increasing the angular displacement causes the actuator of the joint to move the link connected to it within the workspace at a specific time. The two curves in the figure show that the robot moves with high speed and high precision.

(a) Actuator 1   (b) Actuator 2
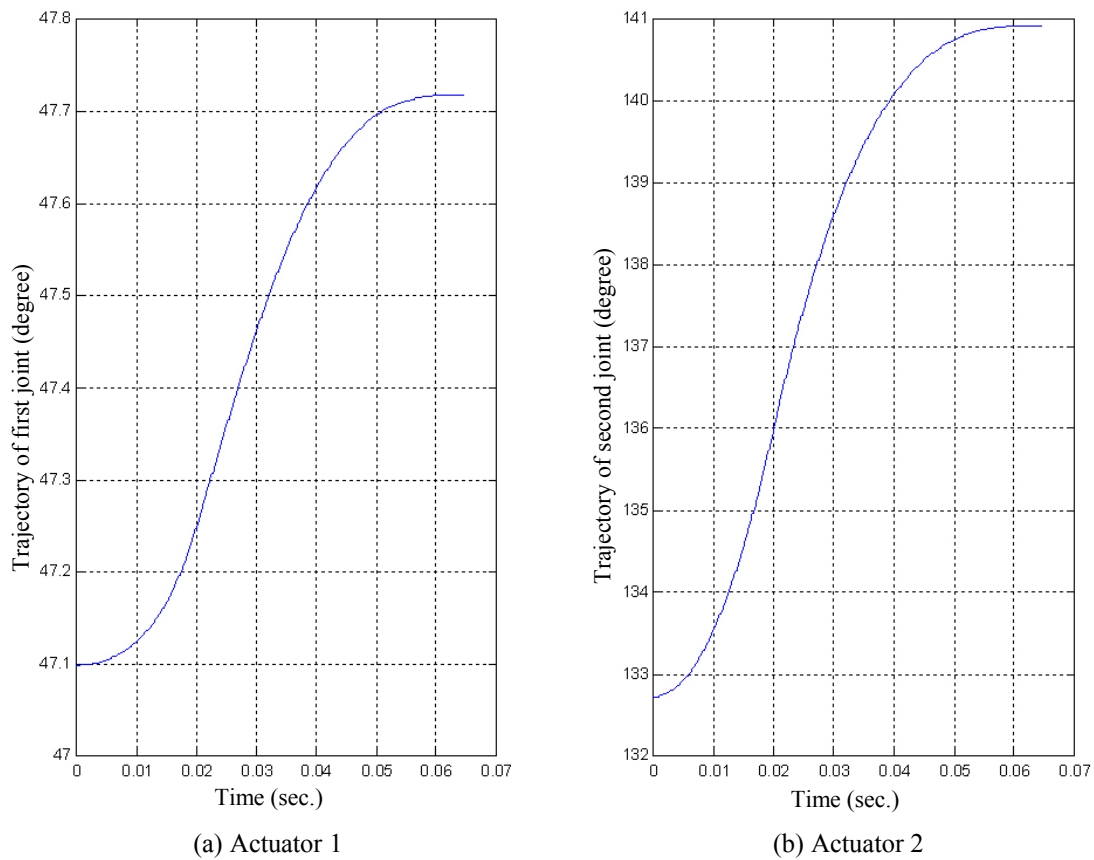
Figure 5. Trajectory generation for the actuators

The displacement curve for the end-effector is obtained (Figure 6) by using (x_p, y_p) that represents the moving platform from equation 8, then selecting different displacements within the workspace area with respect to time, and implementing them again in the MATLAB program. Figure 6 presents the movement of the end-effector within the workspace at a specific time.
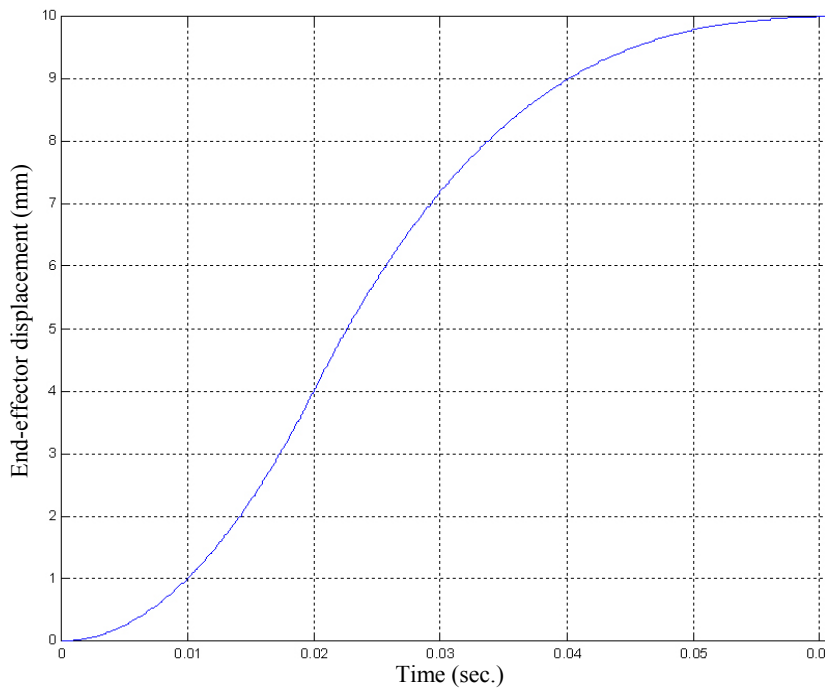
Figure 6. Displacement of the end-effector

SINGULARITY AND WORKSPACE ANALYSIS

Singularity Analysis

From the application point of view, limited workspace and complicated singularities are the two major drawbacks of parallel robots. Singularity refers to configurations in which a parallel robot either loses or gains one or more degrees of freedom instantaneously. In other words, if a parallel robot is in a singular configuration, it will lose its designated motion and working capability and will split its already limited workspace into several rather small regions [27, 28].

The mechanical structure of the proposed robot was designed to release several singularities through the existence of the parallelogram part, as shown in Figure 7.

(a) links 3, 4 in co-linear   (b) links 1, 3 and 2,4 in co-linear   (c) links 3, 4 in co-linear vertically
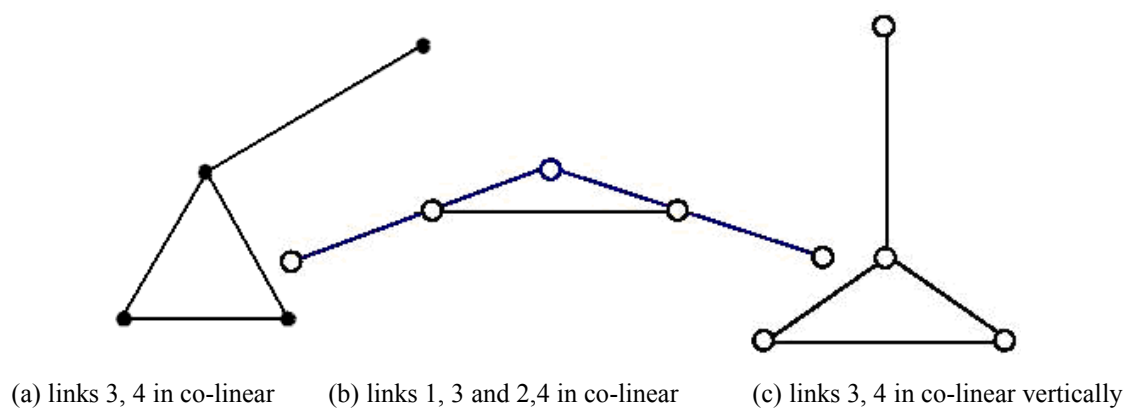
Figure 7. Released singularity by parallelogram device

These released singularities cannot occur because of mechanical constraints. As shown in Figure 7(a) the third and fourth links cannot be in a co-linear position. In Figure 7(b) the first and third

links and the second and fourth links cannot be in a co-linear position. In Figure 7(c) the third and fourth links cannot be in a co-linear position vertically because of the existence of the parallelogram part.

Although several singularities are released, other singularities still occur in the workspace of the robot, making it work in a limited workspace. As shown in Figure 8(a), a singularity occurs when $\theta_2 = \theta_{EC}$. In Figure 8(b) a singularity occurs when $\theta_1 = \theta_{AC}$ (note from Figure 3 that $\theta_{AC} = \theta_1 + \gamma$). In Figure 8(c) a singularity occurs when $\theta_1 = \theta_{AC}$ and $\theta_2 = \theta_{EC}$, which indicates a double singularity.
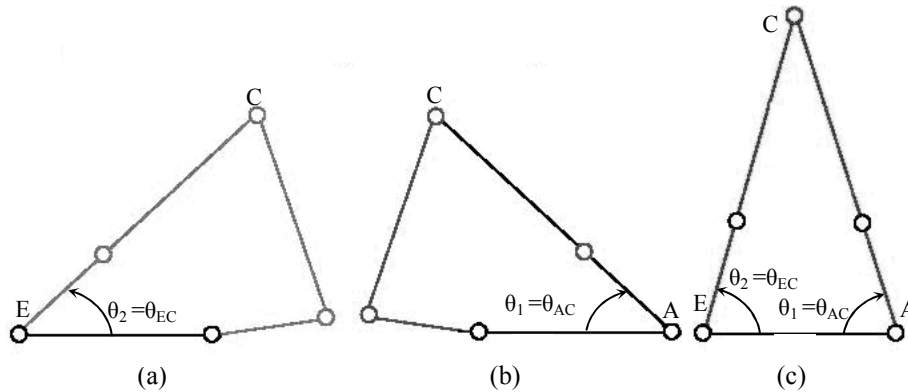
Figure 8. Singularities that must be considered and avoided

Therefore, the value of the input joint in the controlling process must be $\theta_1 < \theta_{AC}$ and $\theta_2 > \theta_{EC}$ to avoid singularities and allow the robot to reach all the workspace positions. This singularity condition must be avoided and carefully considered when the system is implemented.

Workspace Analysis

The workspace of the 2-DOF planar parallel manipulator includes all reachable positions of the end-effector, using all available input motions [29, 30]. However, for parallel manipulators, numerical methods and computer implementation are the only means of representing and displaying the workspace.

The detailed geometric and kinematic properties of the kinematic manipulator structure play an important role in the range of manipulation tasks that can be performed by the robot. The parameters of the links, base and mobile platform should be designed to optimise the workspace.

Our robot can work with the angle of the input joint in the range of ($10°<\theta_1<170°$) and ($10°<\theta_2<170°$) with respect to the mechanical structure (because of the singularity discussed in the previous section). This workspace depends on the length of the first link (l_1) and the ratio of the lengths of the third to the first link ($\delta = l_3/l_1$). In our robot the optimum design for the links is $l_1 = 70$ mm and $\delta = 1.4–1.6$.

As previously illustrated, the function of this robot is for MEMS and IC bonding. Therefore, the workspace of the robot must cover the area of the chip (65×65 mm^2). The workspace of the robot required to achieve this goal is shown in Figure 9. The chip area and workspace are covered and tested in the prototype implementations and experimental part.
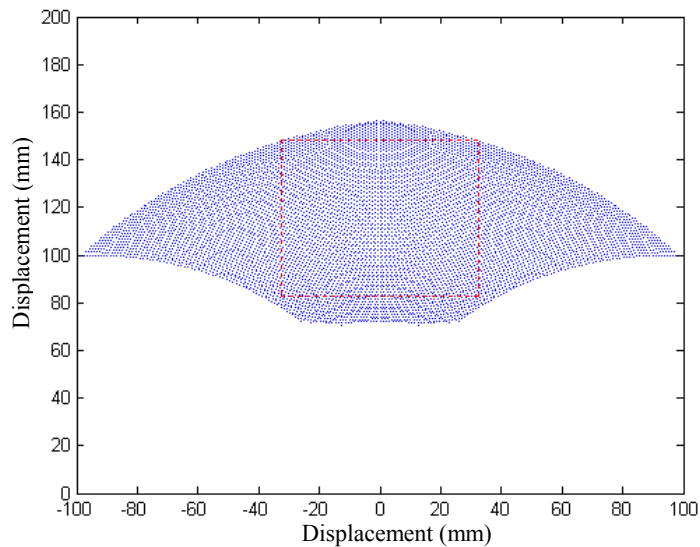
Figure 9. Workspace of the robot

DYNAMIC MODEL

Two approaches are employed to determine the dynamic equations and these are Newton-Euler and Lagrangian's formulation, which are basically equivalent [31, 32]. In Lagrange's methods (which are more tractable and systematic), the Lagrangian L is defined as the difference between kinetic energy K and potential energy P of the system:

$$L = K - P \ . \tag{20}$$

The dynamic equations are obtained as:

$$\tau_j = \frac{d}{dt}\left(\frac{\partial L}{\partial \dot{\theta}_j}\right) - \frac{\partial L}{\partial \theta_j} \ . \tag{21}$$

Given that the potential energy of our robot is constant, the formulation is simplified with the format:

$$\tau_j = \frac{d}{dt}\left(\frac{\partial K}{\partial \dot{\theta}_j}\right) - \frac{\partial K}{\partial \theta_j} \ , \tag{22}$$

where

$$\frac{d}{dt}\left(\frac{\partial K}{\partial \dot{\theta}_j}\right) = \sum_{i=1}^{7}\sum_{k=1}^{2}\left[Tr(U_{ij}J_iU_{ik}^T)\ddot{\theta}_k\right] + 2\sum_{i=1}^{7}\sum_{k=1}^{2}\left[Tr(\dot{U}_{ij}J_iU_{ik}^T)\dot{\theta}_k\right] \tag{23}$$

and

$$\frac{\partial K}{\partial \theta_j} = \sum_{i=1}^{7}\sum_{k=1}^{2}\sum_{p=1}^{2}\left[Tr(\dot{U}_{ij}J_iU_{ip}^T)\dot{\theta}_k\dot{\theta}_p\right] \ , \tag{24}$$

where

$$U_{ij} = \frac{\partial^0 T_i}{\partial \theta_j} \tag{25}$$

and

$$\dot{U}_{ij} = \frac{\partial(U_{ij})}{\partial \theta_1}\dot{\theta}_1 + \frac{\partial(U_{ij})}{\partial \theta_2}\dot{\theta}_2 \ . \tag{26}$$

We substitute $\frac{d}{dt}(\frac{\partial K}{\partial \dot{\theta}_j})$ and $\frac{\partial K}{\partial \theta_j}$ into equation 22 to obtain the torque values.

We simulated these equations with a computer program to obtain the output torque curves for the two actuators in transient time. The curves are shown in Figure 10. These curves are important for the selection of the motors to satisfy the maximum torque for the loads.

(a) Actuator-1 torque   (b) Actuator-2 torque
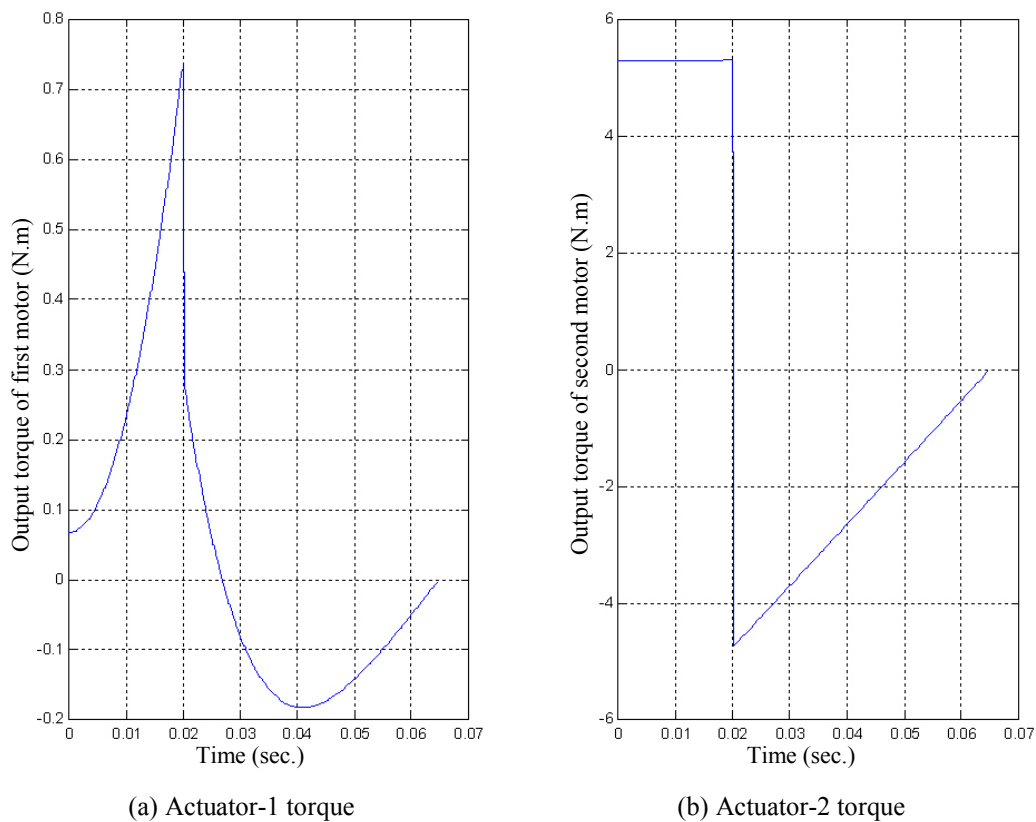
Figure 10. Simulation results for torque of motors

## CONTROL AND EXPERIMENTAL RESULTS

The proposed robot should work in real time. Therefore, onboard programming is needed to prevent an interruption from occurring in the host computer. A National Instruments motion control card (7344) was selected. The actuator control was a direct-drive motor driven by an amplifier motor driver. A software is also required to serve as an interface between the computer and motion control card. LabVIEW and FlexMotion were used to perform this task [33, 34]. The control algorithm was built in LabVIEW by using the FlexMotion coded system. FlexMotion is a separate virtual instrument library for use with LabVIEW. Figure 11 shows the FlexMotion program codes in LabVIEW.
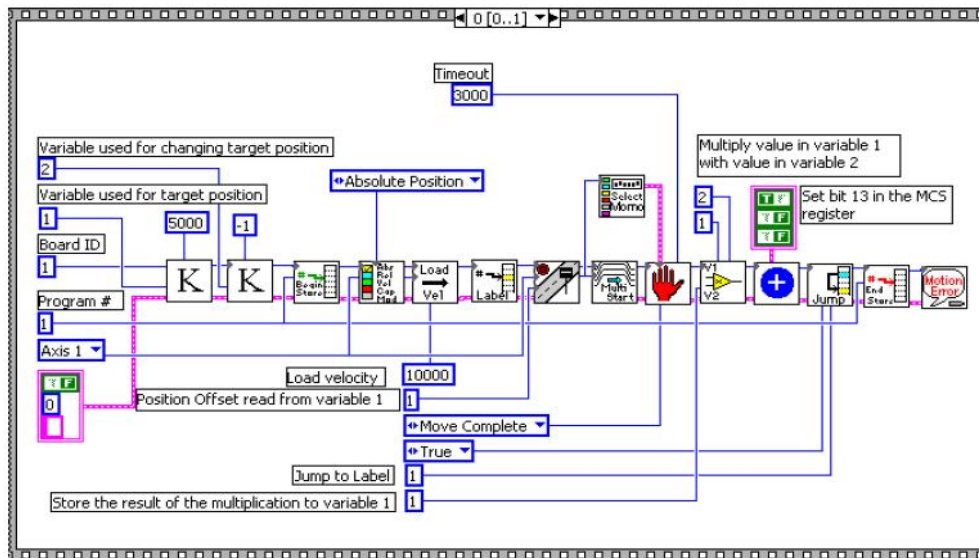
Figure 11. FlexMotion program codes in LabVIEW

The National Instruments (NI 7344) motion control card [35] was used for the controlling process of the manipulator as an upper control system, and DYNASERV was utilised to drive the manipulator motors [36]. The DYNASERV amplifier motor driver was adopted to drive the manipulator motors in direct-drive mode. DYNASERV is composed of a motor section incorporated with an encoder and a driver section.

DYNASERV receives the command of the working algorithm from the control card. It is connected to the encoder in a close loop to control the required position of the motor, given that the trajectory plan originates from the controller. Figure 12 presents the connection between the control card and encoder.
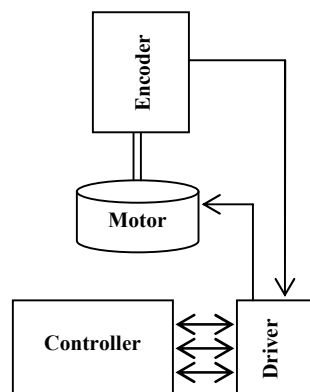

Figure 12. Connection between control card and encoder

The proportional-integral-differential (PID) control algorithm was used to control the system and track the generated trajectory signal. A novel PID control based on the parameter related to the size of the region of interest was developed. The proposed configuration proved that under classical PID control, semi-global stability could be guaranteed with a small output tracking error [37]. Another study based on a model of the robot was presented for the stability of rigid robot arms controlled by PID algorithms. The theoretical results were proven with a simple 2-DOF robot [38]. In another work a nonlinear PID control scheme applied to the complex trajectory tracking control

of a 2PRP-PPR (P-prismatic, R-revolute) planar parallel manipulator with 3-DOF was proposed. The presented experimental results validated the effectiveness of the proposed control scheme [39].

A study also presented a 2-DOF fractional-order PID control scheme for a two-link planar rigid robotic-manipulator trajectory-tracking task. The robustness of the proposed controller was tested to validate the effectiveness of the proposed PID controller. The results revealed that the 2-DOF FOPID controllers were superior to their integer-order counterparts and traditional PID controllers [40]. The possibility of using a PID architecture in robotic 2D navigation systems was also presented in a previous study. The researchers used a developed prototype system implemented for robotic applications that required high-precision movement to follow the control provided for an unmanned, autonomous driving system. The results revealed the effectiveness of the PID controller in enabling the high precision of robotic movements in two dimensions [41].

PID feedback systems are widely used in various applications due to their robustness, accuracy and stability. A PID controller, a control loop feedback controller that is commonly used in control systems, was adopted in the current work to improve the trajectory generation signal and decrease the response time. As shown in Figure 13, the errors between the desired and actual trajectories are sent to the PID controller, which produces the adjustment signal for the motor system. The signals from the encoder are sent back from the closed loop to the desired trajectory unit to determine whether the manipulator reaches the target position. The PID controller continuously calculates the error value as the difference between the desired trajectory tracking and the encoder's measured value to minimize the error over time.
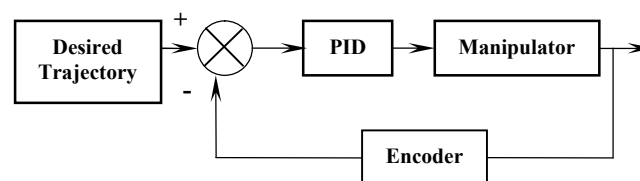
Figure 13. Control algorithm representation

Numerical simulations for conventional PID controllers were conducted with MATLAB/Simulink. The algebraic solver used for the Simulink model was developed from equation 22. The sampling time was maintained at 1 msec. and the torque constraints were limited to [0,10]N.m for the simulation. The controller parameters for the conventional PID controller were obtained as Kp = 5, Ki = 1 and Kd = 40.

The output of the measured step response curve is shown in Figure 14. The unit of the Y axis is represented by counts (every 655,360 counts represent 360 degrees). The target position is 1,000 counts. The X axis represents time.
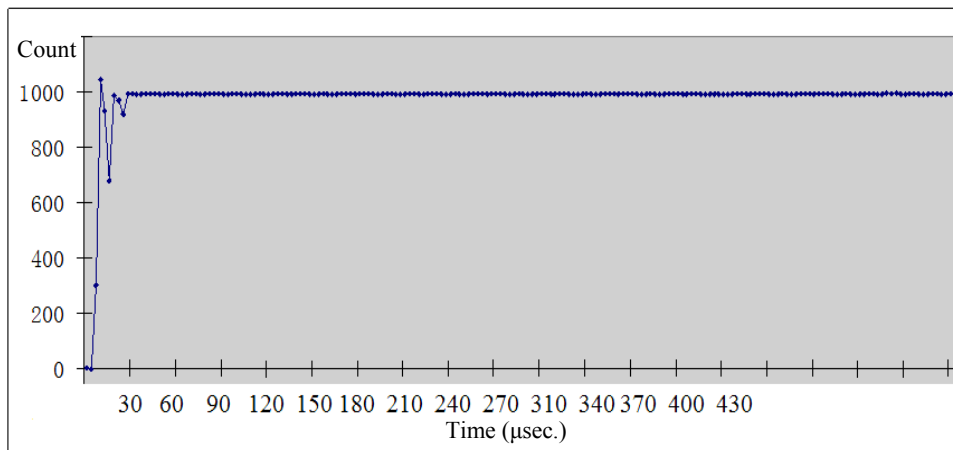
Figure 14. Step response curve

The desired stable duration (i.e. the duration between the first time the motor achieved the target position and the time when it became stable inside a tiny range around the target position, e.g. −1 to +1 count for this system) should be less than 50 μsec. to satisfy this requirement, as shown in Figure 14. Another requirement for precision is that the steady error for the position should be less than 3 counts. For the case shown in Figure 14, the steady error is nearly 0.

The user interface of the debugging program using LabVIEW is shown in Figure 15. The PID parameters used in the experiment and the step response curve are also shown in this figure. To determine the time on the X axis, the value must be multiplied by 3 μsec. The results show that by using a PID controller, the trajectory generation signal improves and the response time decreases.

During the implementation of the proposed prototype robot and experimentation on its functionality, it was observed that the end-effector covered the workspace area of MEMS. In addition, observation also showed that the singularity was avoided exactly in the same manner as it was designed and modelled before.
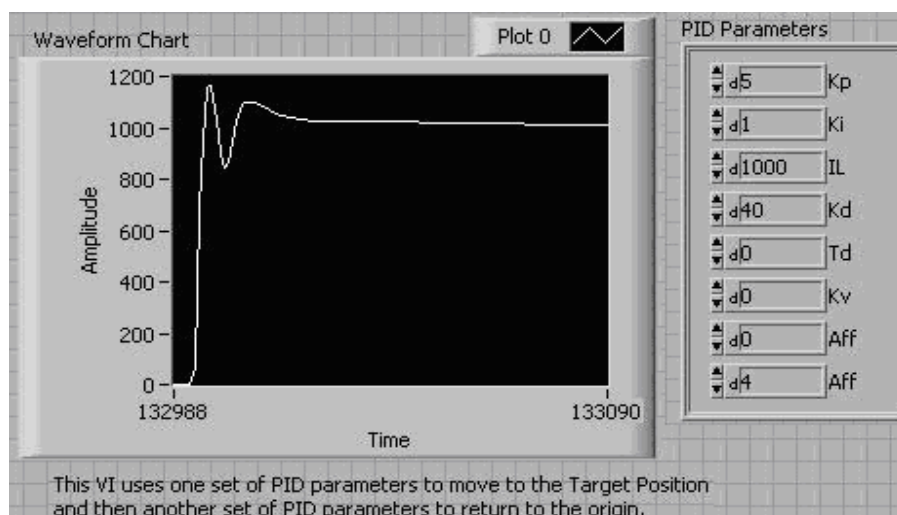
Figure 15. User interface of debugging program

CONCLUSIONS

   A planar parallel manipulator was designed and modelled. The proposed 2-DOF manipulator was analysed to satisfy the manufacturing requirements for MEMS and IC bonding. The forward and inverse kinematics equations for each joint were calculated. Newton-Euler and Lagrangian formulations for the dynamic equation and torque values were determined. Trajectory generation curves for the actuators and displacement curves for the end-effector were obtained. The workspace of the proposed robot was analysed to ensure that the robot can achieve the task requirements of MEMS bonding. The singularities of the mechanical manipulator for each joint were analysed to ensure that the robot avoids mechanical constraints, and the system control was built by using the (NI 7344) motion control card. The experimental results have proved that the robot works in real time with high speed and high acceleration and presents a good response to trajectory generation. The robot covers the workspace field and avoids singularities. By adjusting the PID parameters, the desired stable duration is less than 50 µsec. and the steady-state error is less than 3 counts.

REFERENCES

1.   M. Ganesh, B. Bihari, V. S. Rathore, D. Kumar, C. Kumar, A. R. Sree, K. N. Sowmya and A. K. Dash, "Determination of the closed-form workspace area expression and dimensional optimization of planar parallel manipulators", *Robot.*, **2017**, *35*, 2056-2075.
2.   F. A. Lara-Molina, E. H. Koroishi and D. Dumur, "Design criteria of 2-DOF planar parallel manipulator with flexible joints", Proceedings of 12th IEEE International Conference on Industry Applications, **2016**, Curitiba, Brazil, pp. 1-6.
3.   J. Bryzek, S. Roundy, B. Bircumshaw, C. Chung, K. Castellino, J. R. Stetter and M. Vestel, "Marvelous MEMs: Advanced IC sensors and microstructures for high volume applications", *IEEE Circuits Devices Magaz.*, **2006**, *22*, 8-28.
4.   J. W. Judy, "Microelectromechanical systems (MEMS): Fabrication, design and applications", *Smart Mater. Struct.*, **2001**, *10*, 1115-1134.
5.   M. W. Miles, "Method for fabricating a structure for a microelectromechanical systems (MEMS) device", *U.S. Patent* 6,794,119B2 (**2004**).
6.   J. C. Christenson, S. E. Staller, J. E. Freeman, T. A. Chase, R. L. Healton and D. B. Rich, "MEMS sensor structure and microfabrication process therefor", *U.S. Patent* 6,428,713 (**2002**).
7.   M. Renaud, K. Karakaya, T. Sterken, P. Fiorini, C. V. Hoof and R. Puers, "Fabrication, modelling and characterization of MEMS piezoelectric vibration harvesters", *Sens. Actuat. A Phys.*, **2008**, *145*, 380-386.
8.   Y. T. Cheng, L. Lin and K. Najafi, "Localized silicon fusion and eutectic bonding for MEMS fabrication and packaging", *J. Microelectromech. Syst.*, **2000**, *9*, 3-8.
9.   J. W. F. Cheung and Y. S. Hung, "Modelling and control of a 2-DOF planar parallel manipulator for semiconductor packaging systems", Proceedings of International Conference on Advanced Intelligent Mechatronics, **2005**, Monterey (CA), USA, pp.717-722.
10. X. J. Liu, J. Li and Y. Zhou, "Kinematic optimal design of a 2-degree-of-freedom 3-parallelogram planar parallel manipulator", *Mechan. Machine Theory*, **2015**, *87*, 1-17.
11. M. J. D. Hayes, "Architecture independent workspace analysis of planar three-legged manipulators", Proceedings of Workshop on Fundamental Issues and Future Research Directions for Parallel Mechanisms and Manipulators, **2002**, Quebec, Canada, pp.1-10.

12. O. Mori and T. Omata, "Coupling of two 2-link robots with a passive joint for reconfigurable planar parallel robot", Proceedings of IEEE International Conference on Robotics and Automation, **2002**, Washington, D.C., USA, pp. 4120-4125.

13. C. M. Gosselin and M. Jean, "Determination of the workspace of planar parallel manipulators with joint limits", *Robot. Auton. Syst.*, **1996**, *17*, 129-138.

14. A. Karger, "Architecture singular planar parallel manipulators", *Mechan. Machine Theory*, **2003**, *38*, 1149-1164.

15. Ş. Staicu, "Kinematics of the 3-RRR planar parallel robot", *UPB Sci. Bull. Ser. D: Mech. Eng.*, **2008**, *70*, 3-14.

16. J. Wu, X. Chen, T. Li and L. Wang, "Optimal design of a 2-DOF parallel manipulator with actuation redundancy considering kinematics and natural frequency", *Robot. Comput. Integr. Manuf.*, **2013**, *29*, 80-85.

17. V. Vinoth, Y. Singh and M. Santhakumar, "Indirect disturbance compensation control of a planar parallel (2-PRP and 1-PPR) robotic manipulator", *Robot. Comput. Integr. Manuf.*, **2014**, *30*, 556-564.

18. A. Doroudchi, M. Heydarzadeh, M. T. Masouleh and M. M. Esfandabad, "An experimental study on open-loop position and speed control of a 3-RRR planar parallel mechanism", Proceedings of 3rd International Conference on Robotics and Mechatronics, **2015**, Tehran, Iran, pp.176-181.

19. M. Özsipahi and E. Söylemez, "On the accuracy analyses of a class of 2-DOF planar parallel manipulators", *Mechan. Transm. Appl.*, **2015**, *31*, 41-48.

20. R. Balan, V. Matieş, S. D. Stan and C. Lapuşan, "Mechatronic concepts in design and control of a 3-RRR micro parallel robot", Proceedings of 4th International Federation of Automatic Control Conference on Management and Control of Production and Logistics, **2007**, Sibiu, Romania, pp.283-288.

21. F. A. Lara-Molina, J. M. Rosario and D. Dumur, "Multi-objective design of parallel manipulator using global indices", *Open Mech. Eng. J.*, **2010**, *4*, 37-47.

22. X. R. Zhu, H. P. Shen and W. Zhu, "Realization and simulation of motion trajectory of a 2-DOF planar parallel manipulator", *Key Eng. Mater.*, **2011**, *467-469*, 1351-1356.

23. P. Ji and H. Wu, "An efficient approach to the forward kinematics of a planar parallel manipulator with similar platforms", *IEEE Trans. Robot. Automat.*, **2002**, *18*, 647-649.

24. Y. Singh, V. Vinoth, Y. R. Kiran, J. K. Mohanta and S. Mohan, "Inverse dynamics and control of a 3-DOF planar parallel (U-shaped 3-PPR) manipulator", *Robot. Comput. Integr. Manuf.*, **2015**, *34*, 164-179.

25. J. Wu, T. Li, X. Liu and L. Wang, "Optimal kinematic design of a 2-DOF planar parallel manipulator", *Tsinghua Sci. Technol.*, **2007**, *12*, 269-275.

26. D. T. Pham and S. Yildirim, "Control of the trajectory of a planar robot using recurrent hybrid networks", *Int. J. Machine Tools Manuf.*, **1999**, *39*, 415-429.

27. G. Yang, W. Chen and I. M. Chen, "A geometrical method for the singularity analysis of 3-RRR planar parallel robots with different actuation schemes", Proceedings of International Conference on Intelligent Robots and Systems, **2002**, Lausanne, Switzerland, pp.2055-2060.

28. C. Li, Theingi and I. M. Chen, "Cases study on the singularity of five-bar planar mechanism with differential gear drives", Proceedings of 6th International Conference on Engineering Design and Automation, **2002**, Maui, Hawaii, pp.399-404.

29. J. J. Cervantes-Sánchez and J. G. Rendón-Sánchez, "A simplified approach for obtaining the workspace of a class of 2-DOF planar parallel manipulators", *Mechan. Machine Theory*, **1999**, *34*, 1057-1073.

30. F. Gao, X. Zhang, Y. Zhao and H. Wang, "A physical model of the solution space and the atlas of the reachable workspace for 2-DOF parallel planar manipulators", *Mechan. Machine Theory*, **1996**, *31*, 173-184.

31. B. Dasgupta and P. Choudhury, "A general strategy based on the Newton–Euler approach for the dynamic formulation of parallel manipulators", *Mechan. Machine Theory*, **1999**, *34*, 801-824.

32. W. J. Book, "Recursive Lagrangian dynamics of flexible manipulator arms", *Int. J. Robot. Res.*, **1984**, *3*, 87-101.

33. W. A. Salah, A. B. Musa, B. A. Zneid, A. A. Sneineh and M. S. Jadin, "Implementation of virtual instruments as a power quality analysis tool", *J. Low Power Electron.*, **2016**, *12*, 83-90.

34. National Instruments, "Motion Control, FlexMotion Software Reference Manual", National Instruments Corporation, Austin (TX), **1999**.

35. National Instruments, "Motion Control, 7344/7334 Hardware User Manual", National Instruments Corporation, Austin (TX), **2001**.

36. National Instruments, "Motion Control, NI-Motion User Manual", National Instruments Corporation, Austin (TX), **2003**.

37. I. Cervantes and J. Alvarez-Ramirez, "On the PID tracking control of robot manipulators", *Syst. Control Lett.*, **2001**, *42*, 37-46.

38. P. Rocco, "Stability of PID control for industrial robot arms", *IEEE Trans. Robot. Automat.*, **1996**, *12*, 606-614.

39. P. S. Londhe, Y. Singh, M. Santhakumar, B. M. Patre and L. M. Waghmare, "Robust nonlinear PID-like fuzzy logic control of a planar parallel (2PRP-PPR) manipulator*", ISA Trans.*, **2016**, *63*, 218-232.

40. R. Sharma, P. Gaur and A. P. Mittal, "Performance analysis of 2-DOF fractional order PID controllers for robotic manipulator with payload", *ISA Trans.*, **2015**, *58*, 279-291.

41. K. K. Lekkala and V. K. Mittal, "PID controlled 2D precision robot", Proceedings of International Conference on Control, Instrumentation, Communication and Computational Technologies, **2014**, Kanyakumari, India, pp.1141-1145.

APPENDIX

Table 1. Description of parameters in Figures 3 and 4

Parameter / constant	Description	Unit
A, B, D, and E	Passive joint names	-
F and G	Joint names	-
C	Position of the end-effector joint	-
θ_1 and θ_2	Driving angles for joints A and E	degree
θ_3 and θ_4	Driving angles for joints B and D	degree
θ_t	Orientation angle of segment BG	degree
(x_1,y_1)	Coordinate position for point A in reference to origin O	metre
(x_2,y_2)	Coordinate position for point E in reference to origin O	metre
(x_3,y_3)	Coordinates for joint B in reference to origin O	metre
(x_4, y_4)	Coordinates for joint D in reference to origin O	metre
(x_p, y_p)	Coordinates for point C in reference to origin O	metre
e	Distance from the origin of the base to joint A or E	metre
l_1	Length between joint AB or ED	metre
l_2	Length between joint CD or CB	metre
l_3, l_4 and l_5	Length of sides BF, FG, and BG	metre
d_1	Length between joint AC	metre
d_2	Length between joint EC	metre
d_{34}	Length between joint BD	metre
α	Angle between e and d_1	degree
β	Angle between e and d_2	degree
γ	Angle between l_1 and d_1	degree
δ	Angle between l_1 and d_2	degree